Two New Mixed-Valence Iron Phosphates Templated by Piperazine: $(C_4H_{12}N_2)[Fe_4(OH)_2(HPO_4)_5]$ and $(C_4H_{11}N_2)_{0.5}[Fe_3(HPO_4)_2(PO_4)(H_2O)]$

Vítezslav Zima† and Kwang-Hwa Lii*

Institute of Chemistry, Academia Sinica, Taipei, Taiwan 115, R.O.C.

Ninh Nguyen and Annie Ducouret

Laboratoire CRISMAT-ISMRA, 14050 CAEN Cedex, France

Received February 10, 1998. Revised Manuscript Received April 30, 1998

Two piperazine-templated iron phosphates, $(C_4H_{12}N_2)[Fe_4(OH)_2(HPO_4)_5]$ (**1**) and $(C_4H_{11}N_2)_{0.5}[Fe_3(HPO_4)_2(PO_4)(H_2O)]$ (**2**), have been synthesized under solvothermal conditions and characterized by single-crystal X-ray diffraction, Mössbauer spectroscopy, and thermogravimetric analysis. Compound **1** crystallizes in the monoclinic space group *C*2/*m* (no. 12) with $a = 25.706(3)$, $b = 6.4492(6)$, $c = 6.3790(6)$ Å, $\beta = 102.601(2)°$, $V = 1032.0(3)$ Å^3 and $Z = 2$. The 3-D framework structure consists of layers of iron phosphate which are pillared through HPO_4 groups to generate intersecting 8-ring channels with piperazinium dications at the intersections of these channels. Each layer contains infinite chains of edge-sharing $Fe^{II}O_6$ octahedra which are connected to each other via corner-sharing $Fe^{III}O_6$ octahedra and HPO_4 groups. Compound **2** crystallizes in the monoclinic space group *C*2/*c* (no. 15) with $a = 30.8924(4)$, $b = 6.3733(1)$, $c = 12.5552(2)$ Å, $\beta = 101.946(1)°$, $V = 2418.41(7)$ Å^3, and $Z = 8$. The compound has a layered structure with piperazinium monocations in the interlayer space. Each layer consists of a dimer of edge-sharing octahedra with the composition $Fe^{II}Fe^{III}O_{10}$ which shares edges with four $Fe^{II}O_5$ trigonal bipyramids to form a hexamer as the building unit. Each such hexamer is connected to others by corner sharing and through phosphate groups. Both compounds are mixed-valence as indicated from bond valence calculations, Mössbauer measurements, and electric field gradient calculations.

Introduction

Phosphates of transition metals with open structures represent an interesting group of materials with potential catalytic applications. Organic diamines are often used in the hydrothermal synthesis of these materials as structure-governing components. The first such metallophosphates were prepared with vanadium and molybdenum.[1,2] Recently, a number of works dealing with organically templated iron phosphates have evidenced a rich structural chemistry in this system.[3−5] The choice of organic guest molecules often has a profound influence on the final structure of the material. It appears that diamines with two-carbon chain(s) between nitrogen atoms such as ethylenediamine, piperazine, and 1,4-diazabicyclo[2,2,2]octane (DABCO) are versatile structure-directing agents. As regards templated iron phosphates and oxyfluorinated phosphates, three of them were prepared with ethylenediamine[6−8] and three with DABCO.[9−11] Recently, we have prepared one piperazine-templated iron(III) phosphate by hydrothermal synthesis under acidic conditions.[12] In this paper, we present two other piperazine-templated iron phosphates, $(C_4H_{12}N_2)[Fe_4(OH)_2(HPO_4)_5]$ and $(C_4H_{11}N_2)_{0.5}[Fe_3(HPO_4)_2(PO_4)(H_2O)]$, and show through bond valence calculations, Mössbauer measurements, and electric field gradient calculations that they are mixed-valence compounds.

Experimental Section

Synthesis and Initial Characterization. All syntheses were carried out in Teflon-lined acid digestion bombs with an internal volume of 23 cm^3 under autogenous pressure by heating the starting mixtures at 180 °C for 3 days.

† On leave from Joint Laboratory of Solid State Chemistry, University of Pardubice, 533 14 Pardubice, Czech Republic.

* To whom correspondence should be addressed.

(1) Haushalter, R. C.; Mundi, L. A. *Chem. Mater.* **1992**, *4*, 31 and references therein.

(2) Khan, M. I.; Meyer, L. M.; Haushalter, R. C.; Schweitzer, A. L.; Zubieta, J.; Dye, J. L. *Chem. Mater.* **1996**, *8*, 43 and references therein.

(3) Cavellec, M.; Riou, D.; Greneche, J.-M.; Ferey, G. *Inorg. Chem.* **1997**, *36*, 2181 and references therein.

(4) DeBord, J. R. D.; Reiff, W. M.; Warren, C. J.; Haushalter, R. C.; Zubieta, J. *Chem. Mater.* **1997**, *9*, 1994 and references therein.

(5) Lii, K.-H.; Huang, Y.-F. *J. Chem. Soc., Chem. Commun.* **1997**, 1311 and references therein.

(6) Cavellec, M.; Riou, D.; Ferey, G. *Acta Crystallogr.* **1995**, *C51*, 2242.

(7) DeBord, J. R. D.; Reif, W. M.; Haushalter, R. C.; Zubieta, J. *J. Solid State Chem.* **1996**, *125*, 186.

(8) Huang, C.-Y.; Wang, S.-L.; Lii, K.-H. *J. Porous Mater.* **1998**, *5*, 141.

(9) Lii, K.-H.; Huang, Y.-F. *J. Chem. Soc., Dalton Trans.* **1997**, 2221.

(10) Cavellec, M.; Riou, D.; Ninclaus, C.; Greneche, J.-M.; Ferey, G. *Zeolites* **1996**, *17*, 250.

(11) Cavellec, M.; Riou, D.; Greneche, J.-M.; Ferey, G. *Mater. Res. Soc. Symp. Proc.* **1996**, *57*, 431.

(12) Zima, V.; Lii, K.-H. *J. Solid State Chem.* (in press).

S0897-4756(98)00082-9 CCC: $15.00
Published on Web 06/23/1998

Compound **1,** $(C_4H_{12}N_2)[Fe_4(OH)_2(HPO_4)_5]$, was prepared from a reaction mixture of $FeCl_3 \cdot 6H_2O$ (1 mmol), $FeCl_2 \cdot 4H_2O$ (1 mmol), H_3PO_4 (13 mmol), piperazine (6 mmol), and 9 mL of a mixture of water and ethylene glycol (volume ratio 1:1). The product, containing brown plate crystals, was monophasic as indicated by the excellent agreement of the X-ray powder pattern with that simulated from the atomic coordinates derived from single-crystal study. The yield was 45% based on iron. A plate crystal was chosen for single-crystal X-ray structure determination.

Compound **2**, $(C_4H_{11}N_2)_{0.5}[Fe_3(HPO_4)_2(PO_4)(H_2O)]$, was prepared from a less acidic solution of $FeCl_3 \cdot 6H_2O$ (0.5 mmol), $FeCl_2 \cdot 4H_2O$ (1.5 mmol), H_3PO_4 (6 mmol), piperazine (6 mmol), and 9 mL of a mixture of water and ethylene glycol (1:1 in volume). The product was a mixture of compound **1**, in the form of a fine powder, and dark green platelets, compound **2**, which were manually separated with the aid of ultrasound. The X-ray powder pattern of the powdered sample of the dark green platelets agreed well with that calculated from single-crystal data. The yield of **2** was 41% based on iron.

Elemental analysis proved the amount of piperazine in both compounds according to the formula proposed. Found for compound **1**: C, 6.05; H, 2.27; N, 3.22%. Theoretical: C, 5.81; H, 2.42; N, 3.39%. Found for **2**: C, 4.71; H, 1.60; N, 2.65%. Theoretical: C, 4.65; H, 1.84; N, 2.71%. Energy-dispersive X-ray fluorescence analysis using a JEOL analytical electron microscope confirmed the presence of Fe and P but no Cl in both compounds. Thermogravimetric analyses were performed on a Perkin-Elmer TGA 7 thermal analyzer. The samples were heated to 900 °C at 10 °C min^{-1} in air. The products of heating were identified by powder X-ray diffraction.

Single-Crystal X-ray Diffraction. Crystals of dimensions 0.05 × 0.1 × 0.3 mm (compound **1**) and 0.04 × 0.3 × 0.4 mm (**2**) were used for indexing and intensity data collection on a Siemens Smart-CCD diffractometer equipped with a normal-focus, 3-kW sealed-tube X-ray source. Intensity data were collected in 1271 frames for both **1** and **2** with increasing ω (width of 0.3° per frame). Number of measured and observed reflections ($F_o > 4\sigma(F_o)$): 6303, 1061 for **1**; 13744, 2305 for **2**. Agreement between equivalent reflections (R_{int}): 0.0456 for **1** and 0.0418 for **2**. Empirical absorption corrections were applied by using the SADABS program for the Siemens area detector ($T_{min,max}$: 0.712, 0.942 for **1**; 0.726, 0.928 for **2**). On the basis of systematic absences, statistics of intensity distribution and successful solution and refinement of the structures, the space groups were determined to be *C*2/*m* (no. 12) for **1** and *C*2/*c* (No.15) for **2**. The structure was solved by direct methods: the metal and phosphorus atoms were first located, and the oxygen, nitrogen, and carbon atoms were found in difference Fourier maps. Hydrogen atoms were not located. For **1**, HP(3)O_4 is disordered over four positions. P(3) is at a general position with an occupancy factor (*f*) of 0.25 and is located near the 2*c* special position with a site symmetry of 2/*m*. Two oxygen atoms, O(7), are on a mirror plane with $f = 1$, O(8) is at a general position with $f = 0.25$, and O(9) sits on a two-fold axis with $f = 0.5$. No constraints on the atomic coordinates and thermal parameters were applied to the atoms of HP(3)O_4 during the structure refinement. The piperazinium cation is disordered between two sites. The final cycles of least-squares refinement including the atomic coordinates and anisotropic thermal parameters for all atoms converged at $R1=0.0409$ for **1** and $R1=0.0402$ for **2**. Neutral-atom scattering factors for all atoms were used. Anomalous dispersion and secondary extinction corrections were applied. Structure solution and refinement were performed by using SHELXTL PC programs.[13]

Mössbauer Spectroscopy. Bond valence calculations clearly indicate that both compounds are mixed valence. To confirm the mixed-valence nature, the powder ^{57}Fe room-temperature Mössbauer spectra were registered in a transmission geometry with a constant acceleration spectrometer using a ^{57}Co source in a Rh matrix. These spectra were fitted by means of the MOSFIT program.[14]

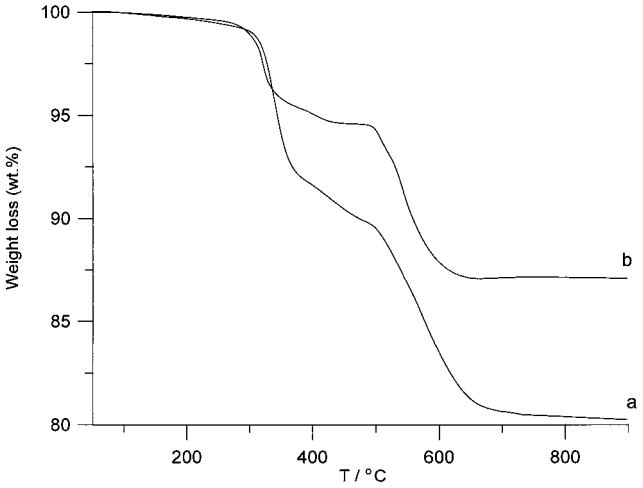

Figure 1. Thermogravimetric analysis of $(C_4H_{12}N_2)[Fe_4(OH)_2(HPO_4)_5]$ (a) and $(C_4H_{11}N_2)_{0.5}[Fe_3(HPO_4)_2(PO_4)(H_2O)]$ (b) in flowing air at 10 °C min^{-1}.

Results and Discussion

Thermogravimetric Analysis. The onset of weight loss occurs at approximately 300 °C for both compounds. A two-step weight loss of 18.68% is observed for **1** in the temperature range of 50−700 °C (Figure 1a). The two steps are not well resolved. On the basis of powder X-ray diffraction, the decomposition product at 400 °C is amorphous. The products at 700 °C are the trivalent iron compounds $Fe_4(P_2O_7)_3$ and $FePO_4$ according to their X-ray powder diffraction pattern.[15] The observed total weight loss agrees well with that calculated for the loss of 20 H_2O and 4 piperazine molecules (18.41%), as indicated from eq 1:

$$4\,(C_4H_{12}N_2)[Fe_4(OH)_2(HPO_4)_5] + 3\,O_2 \rightarrow 2\,Fe_4(P_2O_7)_3 + 8\,FePO_4 + 20\,H_2O + 4\,C_4H_{10}N_2 \quad (1)$$

Water is released in the first step due to the dehydration of OH^- and HPO_4^{2-} groups and deprotonation of the piperazinium dication, and the second step corresponds to the release of the organic component. Elemental analysis of the amorphous product at 400 °C (C, 6.18; H, 0.40; N, 3.50%; C:H:N molar ratio = 2.06:1.6:1) indicated the presence of organic molecules. The smaller content of hydrogen in the product is most probably caused by dehydrogenation of piperazine to pyrazine or to other products of pyrolysis. The thermogravimetric curve of **2** (Figure 1b) shows a weight loss of 12.9% in two steps with a curve shape similar to that for **1**. The theoretical weight loss (12.3%) calculated according to eq 2

$$8\,(C_4H_{11}N_2)_{0.5}[Fe_3(HPO_4)_2(PO_4)(H_2O)] + 5\,O_2 \rightarrow 24\,FePO_4 + 4\,C_4H_{10}N_2 + 18\,H_2O \quad (2)$$

is in good agreement with the experimental value. The intermediate product at 450 °C is mostly $Fe_7(PO_4)_6$.[15]

(13) Sheldrick, G. M. *SHELXTL PC*, version 5; Siemens Analytical X-ray Instruments Inc.: Madison, WI, 1995.

(14) Teillet, J.; Varret, F. Unpublished Mosfit program.

(15) $Fe_4(P_2O_7)_3$, file number 36-318; $FePO_4$, 29-715; $Fe_7(PO_4)_6$, 35-282. Joint Committee on Powder Diffraction Standards, International Centre of Diffraction Data, Swarthmore, PA.

Table 1. Crystallographic Data for $(C_4H_{12}N_2)[Fe_4(OH)_2(HPO_4)_5]$ (1) and $(C_4H_{11}N_2)_{0.5}[Fe_3(HPO_4)_2(PO_4)(H_2O)]$ (2)

	1	**2**
formula	$C_4H_{20}N_2O_{22}P_5Fe_4$	$C_2H_{9.5}NO_{13}P_3Fe_3$
M	825.46	516.07
crystal system	monoclinic	monoclinic
space group	$C2/m$ (no. 12)	$C2/c$ (no. 15)
a, Å	25.706(3)	30.8924(4)
b, Å	6.4492(6)	6.3733(1)
c, Å	6.3790(6)	12.5552(2)
β, deg	102.601(2)	101.946(1)
V, Å^3	1032.0(3)	2418.41(7)
Z	2	8
μ(Mo Kα), cm^{-1}	32.6	40.3
ρ_{calcd}, g·cm^{-3}	2.656	2.835
λ, Å	0.71073	0.71073
T, °C	23	23
$R1$[a]	0.0409	0.0402
$wR2$[b]	0.1114	0.1191
goodness of fit	1.072	1.156
$(\Delta\rho)_{max,min}$, e·Å^{-3}	0.72, −0.72	1.22, 1.16

[a] $R1 = \Sigma||F_o| - |F_c||/\Sigma|F_o|$. [b] $wR2 = \{\Sigma[w(F_o^2 - F_c^2)^2]/\Sigma[w(F_o^2)^2]\}^{1/2}$. $w = 1/[\sigma^2(F_o^2) + (aP)^2 + bP]$, $P = [\max(F_o^2,0) + 2F_c^2]/3$, where $a =$ 0.0617 and $b = 1.11$ for **1**, and $a = 0.0682$ and $b = 5.99$ for **2**.

The final decomposition product, $FePO_4$, was confirmed by powder XRD.

Crystal Structures. The crystallographic data are listed in Table 1. The atomic coordinates and the bond lengths and bond valence sums are given in Tables 2 and 3, respectively.

Compound 1. Both iron atoms are six-coordinated, with Fe(1) being trivalent and Fe(2) divalent. P(1) and P(3) form monohydrogen phosphate groups, as inferred from unsatisfied bond valence sums of 1.09 and 1.07 for O(1) and O(8), respectively. To balance charge, P(2) also forms a HPO_4 group. Two O(4) atoms of the P(2)O_4 tetrahedron share one hydrogen as indicated by the bond valence sum of 1.49 for O(4). The low value of the bond valence sum calculated for O(10) ($\Sigma s = 0.994$) suggests that it is a hydroxo oxygen.

The structure is composed of infinite chains of edge-sharing Fe(2)O_6 octahedra parallel to the [010] direction as shown in Figure 2. O(2) and O(10) form the common edge. O(10) is also coordinated to Fe(1) as a μ_3-hydroxo oxygen. O(2) is bonded to P(1). Two other corners of the HP(1)O_4 group are shared with neighboring Fe(1)-O_6 octahedra, with the remaining hydroxo oxygen being unshared. The HP(2)O_4 tetrahedron forms a bridge over edge-sharing Fe(2)O_6 octahedra in a linarite-type motif[16] which has also been observed in $(NH_3C_2H_4NH_3)_{0.5}$[Fe-$(PO_4)(OH)$].[6,7] The remaining corners of HP(2)O_4 are linked to Fe(1)O_6 of neighboring chains such that sheets in the *bc*-plane are formed. The sheets are pillared through HP(3)O_4 tetrahedra (Figures 3 and 4) by corner sharing with the Fe(1)O_6 octahedra, generating intersecting 8-ring channels parallel to the [001] and [010] directions. Diprotonated piperazinium cations, which are disordered over two sites, reside at the intersections of these channels. Empty 6-ring channels parallel to the [010] direction are also formed in the sheets. The HP(3)O_4 group is disordered over four positions and has two terminal oxygens, O(8) and O(9). The former is a hydroxo oxygen. The latter forms hydrogen bonds with two piperazinium cations, as inferred from the short O···N distance of 2.69 Å.

(16) Hawthorne, F. C. *Acta Crystallogr.* **1994**, *B50*, 481.

Table 2. Atomic Coordinates and Thermal Parameters (Å^2 × 100) for $(C_4H_{12}N_2)[Fe_4(OH)_2(HPO_4)_5]$ (1) and $(C_4H_{11}N_2)_{0.5}[Fe_3(HPO_4)_2(PO_4)(H_2O)]$ (2)

atom	x	y	z	U_{eq}[a]
		Compound **1**		
Fe(1)	0.12524(3)	0	0.6900(1)	0.85(2)
Fe(2)	0.25	0.25	0	1.33(3)
P(1)	0.34411(6)	0	0.3258(2)	1.02(3)
P(2)	0.16108(6)	0	0.2053(2)	1.18(3)
P(3)[b]	0.0051(2)	0.1050(6)	0.4426(6)	1.09(9)
O(1)	0.3233(2)	0	0.5422(7)	2.2(1)
O(2)	0.2948(2)	0	0.1391(6)	1.53(9)
O(3)	0.3765(1)	0.1925(5)	0.3215(4)	1.56(6)
O(4)	0.1984(1)	0.1926(5)	0.2246(5)	1.88(7)
O(5)	0.1320(2)	0	0.3864(6)	1.90(9)
O(6)	0.1214(2)	0	−0.0070(6)	1.74(9)
O(7)	0.0464(2)	0	0.6094(7)	2.1(1)
O(8)[b]	0.0253(4)	0.077(2)	0.225(2)	1.9(3)
O(9)[c]	0	0.332(1)	0.5	2.6(2)
O(10)	0.2085(1)	0	0.7926(6)	1.38(8)
N(1)[c]	0.4772(3)	0.096(2)	0.165(1)	4.5(3)
C(1)	0.4419(4)	0	−0.045(1)	8.3(5)
C(2)[c]	0.5328(4)	0.154(3)	0.133(2)	6.3(5)
		Compound **2**		
Fe(1)	0.24909(2)	0.09537(9)	0.08229(4)	1.04(2)
Fe(2)	0.16132(2)	−0.19787(9)	0.03451(5)	1.33(2)
Fe(3)	0.33478(2)	−0.0469(1)	0.25652(5)	1.33(2)
P(1)	0.34329(3)	0.1779(2)	0.01657(8)	1.01(2)
P(2)	0.24481(3)	0.1102(2)	0.34346(8)	0.92(2)
P(3)	0.41780(4)	−0.2929(2)	0.19075(9)	1.52(3)
O(1)	0.31712(9)	0.0782(5)	0.0965(2)	1.35(6)
O(2)	0.31918(9)	0.3774(5)	−0.0332(2)	1.31(6)
O(3)	0.3907(1)	0.2279(5)	0.0751(2)	1.69(6)
O(4)	0.34538(9)	0.0192(4)	−0.0746(2)	1.31(6)
O(5)	0.2677(1)	0.0654(4)	0.2483(2)	1.39(6)
O(6)	0.27079(9)	0.2886(4)	0.4133(2)	1.14(6)
O(7)	0.24852(9)	−0.0871(5)	0.4167(2)	1.29(6)
O(8)	0.1964(1)	0.1655(5)	0.3038(2)	1.56(6)
O(9)	0.3970(1)	−0.1655(5)	0.2701(3)	2.25(7)
O(10)	0.4641(1)	−0.2073(6)	0.1880(3)	2.67(8)
O(11)	0.4211(1)	−0.5265(5)	0.2266(3)	2.42(7)
O(12)	0.3921(1)	−0.2807(5)	0.0736(3)	2.32(7)
O(13)	0.1484(1)	−0.1670(5)	0.1968(2)	1.94(7)
N(1)	0.4524(1)	−0.0230(7)	0.4685(4)	3.5(1)
C(1)	0.5184(2)	0.2086(8)	0.4947(5)	3.0(1)
C(2)	0.4762(2)	0.1415(9)	0.4183(4)	3.4(1)

[a] U_{eq} is defined as one-third of the trace of the orthogonalized U_{ij} tensor. [b] The occupancy factor is 0.25. [c] The occupancy factor is 0.5.

Compound 2. Bond valence calculations indicate that both Fe(2) and Fe(3) are divalent; Fe(1), O(3), O(8), O(9), O(10), O(11), and O(13) have valence sums of 2.49, 1.26, 1.64, 1.71, 1.24, 1.19 and 0.31, respectively; and all other oxygen atoms have values very close to 2. O-(3) and O(10) are hydroxo oxygens. O(13) is a water oxygen. The valence sums of O(8) and O(11) are satisfied by forming hydrogen bonds with water molecules [O(8)···O(13) = 2.77 Å; O(11)···O(13) = 2.68 Å]. O(9) forms a hydrogen bond with a piperazinium cation [O(9)···N(1) = 2.86 Å]. The mixed-valence nature at the Fe(1) site is confirmed by the Mössbauer spectroscopy study (vide infra). To balance charge, the piperazinium cation, which sits on an inversion center, is monoprotonated. Compound **2** is the most Fe^{II} rich of the organically templated FePO frameworks.

The compound has a layered structure with piperazinium cations in the interlayer space (Figure 5). The basic building unit of each layer is a hexamer which is composed of two FeO_6 octahedra and four FeO_5 trigonal bipyramids (Figure 6). All of these iron−oxygen polyhedra are connected via edge sharing. The core of the

Table 3. Bond Lengths (Å) and Valence Sums (Σs) for $(C_4H_{12}N_2)[Fe_4(OH)_2(HPO_4)_5]$ (1) and $(C_4H_{11}N_2)_{0.5}[Fe_3(HPO_4)_2(PO_4)(H_2O)]$ (2)

Compound **1**			
Fe(1)−O(3)	1.984(3) (2×)	Fe(1)−O(5)	1.982(4)
Fe(1)−O(6)	1.957(4)	Fe(1)−O(7)	1.978(4)
Fe(1)−O(10)	2.098(4)		
Σs(Fe(1)−O) = 2.97			
Fe(2)−O(2)	2.066(2) (2×)	Fe(2)−O(4)	2.185(3) (2×)
Fe(2)−O(10)	2.207(3) (2×)		
Σs(Fe(2)−O) = 1.96			
P(1)−O(1)	1.586(4)	P(1)−O(2)	1.538(4)
P(1)−O(3)	1.499(3) (2×)		
Σs(P(1)−O) = 5.08			
P(2)−O(4)	1.559(3) (2×)	P(2)−O(5)	1.506(4)
P(2)−O(6)	1.507(4)		
Σs(P(2)−O) = 5.03			
P(3)−O(7)	1.461(5)	P(3)−O(7)	1.491(6)
P(3)−O(8)	1.59(1)	P(3)−O(9)	1.520(9)
Σs(P(3)−O) = 5.30			
N(1)−C(1)	1.57(1)	N(1)−C(2)	1.54(1)
C(1)−C(2)	1.37(1)		
Compound **2**			
Fe(1)−O(1)	2.075(3)	Fe(1)−O(2)	2.078(3)
Fe(1)−O(5)	2.053(3)	Fe(1)−O(6)	2.054(3)
Fe(1)−O(7)	2.025(3)	Fe(1)−O(7)	2.076(3)
Σs(Fe(1)−O) = 2.49			
Fe(2)−O(2)	2.131(3)	Fe(2)−O(4)	2.129(3)
Fe(2)−O(6)	2.066(3)	Fe(2)−O(12)	1.913(3)
Fe(2)−O(13)	2.165(3)		
Σs(Fe(2)−O) = 2.02			
Fe(3)−O(1)	2.126(3)	Fe(3)−O(4)	2.085(3)
Fe(3)−O(5)	2.173(3)	Fe(3)−O(8)	2.135(3)
Fe(3)−O(9)	2.039(3)		
Σs(Fe(3)−O) = 1.82			
P(1)−O(1)	1.549(3)	P(1)−O(2)	1.539(3)
P(1)−O(3)	1.530(3)	P(1)−O(4)	1.539(3)
Σs(P(1)−O) = 4.94			
P(2)−O(5)	1.537(3)	P(2)−O(6)	1.554(3)
P(2)−O(7)	1.549(3)	P(2)−O(8)	1.518(3)
Σs(P(2)−O) = 4.94			
P(3)−O(9)	1.527(3)	P(3)−O(10)	1.538(3)
P(3)−O(11)	1.553(3)	P(3)−O(12)	1.522(3)
Σs(P(3)−O) = 4.99			
N(1)−C(1)	1.500(7)	N(1)−C(2)	1.492(7)
C(1)−C(2)	1.514(8)		

hexamer is a dimer of $Fe(1)O_6$ octahedra, in which two O(7) atoms form the shared edge. In addition, two $HP(1)O_4$ groups bridge the $Fe(1)O_6$ octahedra of the dimer. All oxygen atoms of the dimer are bonded to one phosphorus and two iron atoms. Each $Fe(1)O_6$ octahedron shares its two skew edges with $Fe(2)O_5$ and $Fe(3)O_5$ trigonal bipyramids. Fe(2) is coordinated by four phosphate oxygen atoms and one water oxygen. Fe(3) is coordinated by five phosphates. The $P(2)O_4$ tetrahedron forms a bridge over $Fe(2)O_5$ and $Fe(3)O_5$ trigonal bipyramids within a hexamer, with the other two corners being coordinated to the iron atoms of neighboring hexamers. $HP(3)O_4$ is coordinated to Fe(2) and Fe(3) belonging to adjacent hexamers, with P(3)−O(10)H and P(3)−O(11) groups being directed into the interlayer space. These hexamers are also connected via Fe(2)−O(4)−Fe(3) bonds.

Mössbauer Spectroscopy and Electric Field Gradient Calculations. Compound 1. The room-temperature Mössbauer spectrum is shown in Figure 7. The best fit leads to four doublet contributions from Fe^{2+} and Fe^{3+} in octahedral coordination. The isomer shift (IS) values are relative to metallic iron. The results are summarized in Table 4. The A and B contributions are assigned to the more distorted iron site, Fe(2), because they have larger values of quadrupole splittings. Both

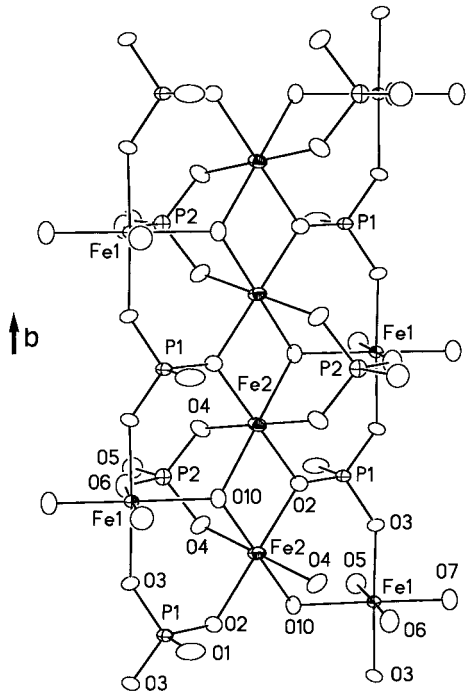

Figure 2. Structural units of $(C_4H_{12}N_2)[Fe_4(OH)_2(HPO_4)_5]$ viewed in a direction approximately parallel to the *c*-axis. Thermal ellipsoids are shown at 60% probability.

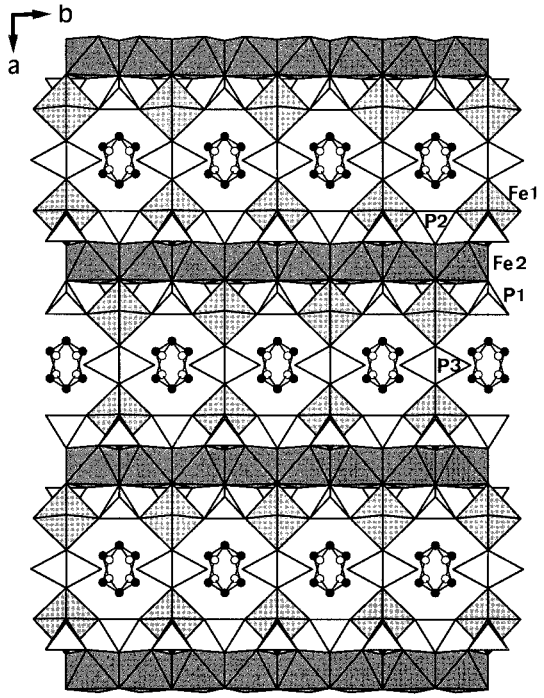

Figure 3. Polyhedral representation of the $(C_4H_{12}N_2)[Fe_4(OH)_2(HPO_4)_5]$ structure viewed along the [001] direction. Octahedra represent FeO_6 groups; tetrahedra, HPO_4; solid circles, C; open circles, N. The $HP(3)O_4$ groups and piperazinium molecules are disordered.

Fe(1) and Fe(2) sites have approximately the same charge distribution: 30% Fe^{2+} and 70% Fe^{3+}. In contrast, bond valence sum calculations based on the results of single-crystal structure analysis clearly indicate that Fe(1) is trivalent and Fe(2) is divalent. The considerable discrepancy between the two results may be rationalized by the presence of isostructural phases with different proton contents in the powder sample for

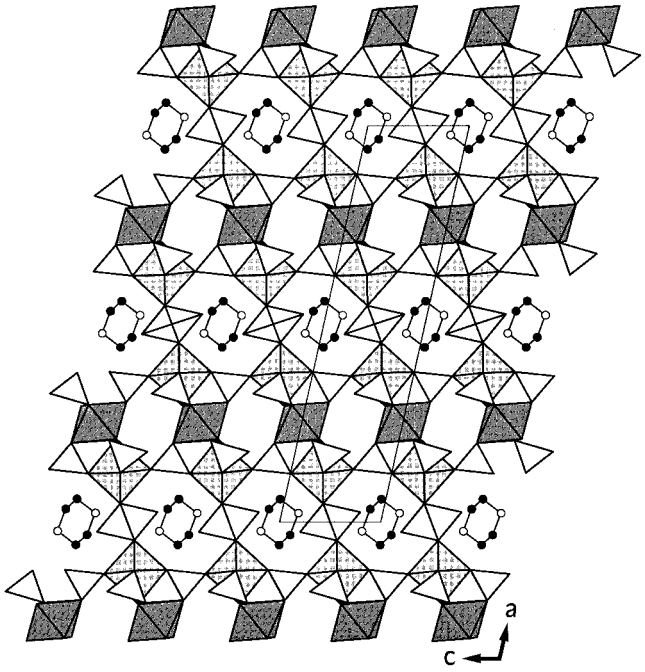

Figure 4. View of the structure of $(C_4H_{12}N_2)[Fe_4(OH)_2(HPO_4)_5]$ along [010].

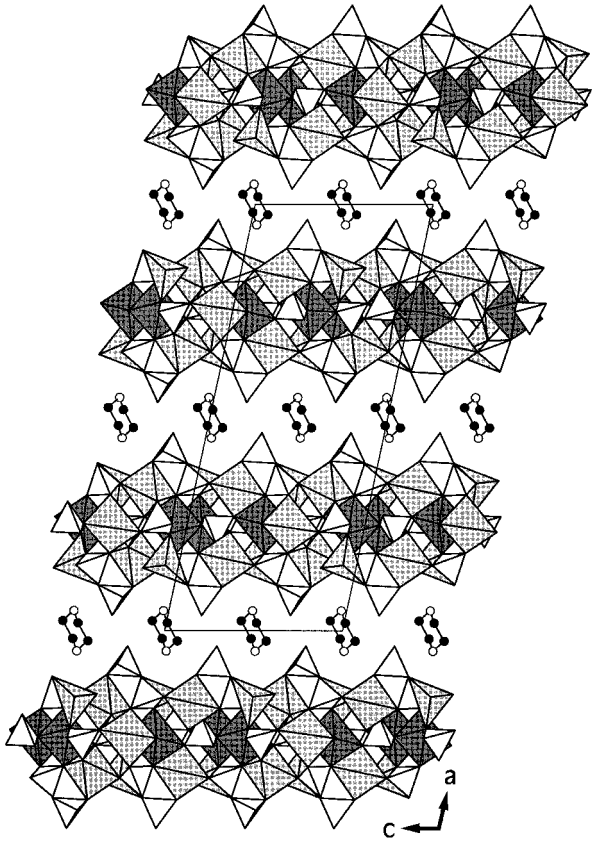

Figure 5. Polyhedral representation of the $(C_4H_{11}N_2)_{0.5}[Fe_3(HPO_4)_2(PO_4)(H_2O)]$ structure viewed along the [010] direction. Polyhedra with darker and lighter shades are FeO_6 octahedra and FeO_5 trigonal bipyramids, respectively; tetrahedra are phosphate groups; solid circles, C; open circles, N.

Mössbauer study. A phase with a smaller proton content is associated with a larger amount of Fe^{3+}. Several isostructural products, which were prepared from gel precursors with different pH values, will be used for further Mössbauer studies.

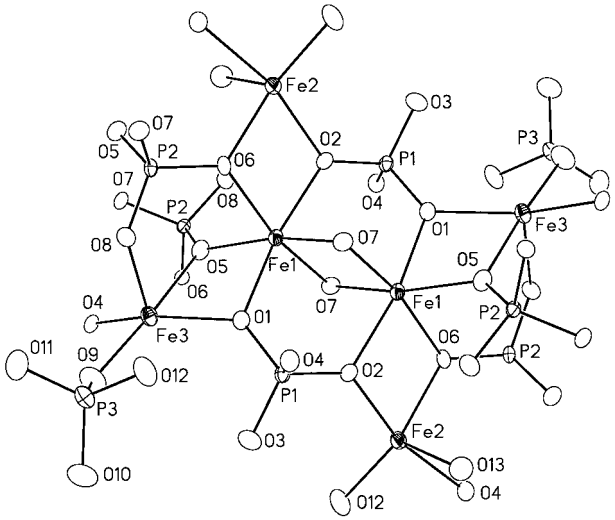

Figure 6. Structural unit of $(C_4H_{11}N_2)_{0.5}[Fe_3(HPO_4)_2(PO_4)(H_2O)]$ viewed along the *c*-axis. Thermal ellipsoids are shown at 60% probability.

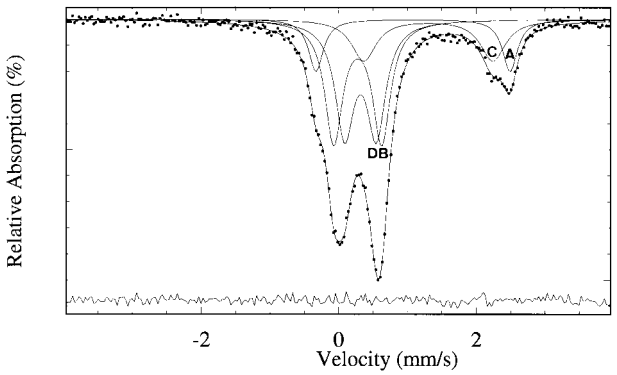

Figure 7. Mössbauer spectrum of $(C_4H_{12}N_2)[Fe_4(OH)_2(HPO_4)_5]$ at 293 K with fitted A−D curves ascribed to the contributions of the Fe^{2+} and Fe^{3+} sites.

Table 4. Isomer Shifts (IS), Absolute Values of Quadrupole Splitting (|QS|) and Relative Spectral Areas (%) of the ^{57}Fe Mössbauer Spectrum Observed at Room Temperature in $(C_4H_{12}N_2)[Fe_4(OH)_2(HPO_4)_5]$

site	IS (± 0.01) (mm s^{-1})	|QS| (±0.02) (mm s^{-1})	iron charge	% (±3)	
A	1.19	2.82	2	13	Fe(2)
B	0.39	0.70	3	35	Fe(2)
C	1.42	1.87	2	17	Fe(1)
D	0.43	0.46	3	35	Fe(1)

Compound 2. The room-temperature Mössbauer spectrum shows that the Fe^{3+}/Fe^{2+} ions are present in a paramagnetic state (Figure 8). The best fit leads to five doublet contributions from Fe^{2+} and Fe^{3+} in octahedral or trigonal bipyramidal coordination. Table 5 gives the fitted experimental results at 293 K. The smaller value of IS at the E site is typical of trivalent iron. The IS values for the A, B, C, and D sites are characteristic of divalent iron. The relative spectral area of 13 ± 5% for Fe^{3+} is in agreement with the result of bond valence calculations ($[Fe^{3+}] = 16.6\%$). The introduction of the C doublet is necessary to obtain a good fit despite its small intensity.

The three crystallographically different iron atoms are present in equal amount. Therefore, the following repartition of the Mössbauer doublets is suggested: D(Fe^{2+}) and E(Fe^{3+}) are at the same iron site ([D] +

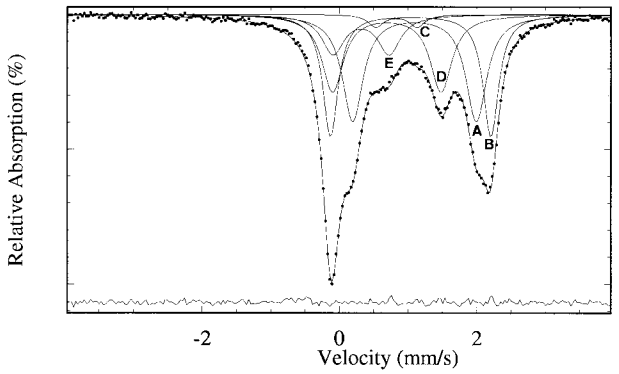

Figure 8. Mössbauer spectrum of $(C_4H_{11}N_2)_{0.5}[Fe_3(HPO_4)_2(PO_4)(H_2O)]$ at 293 K showing the contributions attributed to the Fe^{2+} and Fe^{3+} sites as fitted by curves A−E.

Table 5. Isomer Shifts (IS), Absolute Values of Quadrupole Splitting (|QS|) and Relative Spectral Areas (%) of the ^{57}Fe Mössbauer Spectrum Observed at Room Temperature in $(C_4H_{11}N_2)_{0.5}[Fe_3(HPO_4)_2(PO_4)(H_2O)]$

site	IS (± 0.01) (mm s^{-1})	|QS| (± 0.02) (mm s^{-1})	iron charge	% (± 3)	
A	1.21	1.80	2	32	Fe(3)
B	1.15	2.33	2	28	Fe(2)
C	0.95	0.60	2	3	Fe(2)
D	0.81	1.58	2	24	Fe(1)
E	0.43	0.81	3	13	Fe(1)

[E] = 24% + 13% = 37%), B(Fe^{2+}) and C(Fe^{2+}) are at another site ([B] + [C] = 28% + 3% = 31%), and A(Fe^{2+}) is at the third site by itself (32%).

Among the four major doublets, namely, A, B, D, and E, the D and E contributions have the smallest absolute values of quadrupole splitting, |QS|. Because the quadrupole splitting corresponds to the asymmetrical part of the electric hyperfine interaction between the iron nucleus and the surrounding charges, it can be written as the sum of two terms: $QS = QS^V + QS^l$, where QS^V is the "valence" contribution from the 3d electron shell of iron, and QS^l is the "lattice" contribution due to other ionic charges in the crystal. Both terms reflect the local symmetry of the iron site. The smaller value of QS is associated with higher site symmetry. Therefore, the octahedral Fe(1) site can be assigned to the D and E doublets, which correspond to the highest site symmetry.

In fact, the analysis is more complicated in two ways: (i) Mössbauer fits of powder samples give only the absolute value of QS in the paramagnetic state, and (ii) in some cases, QS^V and QS^l can occur with approximately opposite values despite the asymmetrical character of the site, leading to a small global QS value. Therefore, to better understand the experimental |QS| values and to confirm the assignment of the A, (B+C), and (D+E) doublets, we have performed electric field gradient (EFG) calculations at all three crystallographically different iron sites based on the results of the crystal structure analysis.

For the Fe^{3+} sites, the $3d^5$ valence shell is essentially spherical, $QS^V \approx 0$, and $QS \approx QS^1 = (1 - \gamma_\infty)(eQ/2)V^l_{ZZ}(1 + \eta^2/3)^{1/2}$ where V^l_{ZZ} is the principal component of the $[V^l_{ij}]$ lattice EFG tensor, $\eta = (V_{XX} - V_{YY})/V_{ZZ}$ is the asymmetry parameter ($0 \le \eta \le 1$ if $|V_{ZZ}| \ge |V_{XX}| \ge |V_{YY}|$), Q (≈ 0.2 barn)[17] is the quadrupolar momentum of ^{57}Fe in the excited $I = 3/2$ state, and $(1 - \gamma_\infty)$ is the antishielding Fe^{3+} Sternheimer factor.[18] So, lattice calculations for Fe^{3+} sites give both the sign and the magnitude of the total quadrupole splitting, which can be compared to the experimental results.

Owing to the large number of atoms in a unit cell and the low symmetry of the space group, EFG lattice calculations have not been developed for the whole crystal but are limited to the monopolar contributions of the first neighbors of the Fe^{3+} ion. They lead to QS = 0.76(4) mm s^{-1} and $\eta = 0.4(1)$ if Fe^{3+} is in the Fe(1) site. The same calculations performed on Fe^{3+} with the coordination environments for Fe(2) and Fe(3) give two or three times higher QS values with respect to the experimental result ($|QS|_E = 0.81(2)$ mm s^{-1}). Consequently, the Fe^{3+}(E) contribution can be unambiguously assigned to the octahedral Fe(1) site. Furthermore, the good agreement between the calculated and experimental values indicates that the first oxygen neighbors are the most relevant contribution despite the approximations in the calculations. Note also that the value of QS deviates only ±0.04 mm s^{-1} when more distant atoms up to 3.5 Å are included. In addition, the principal component V^l_{ZZ} for Fe(1) has a positive medium value and is approximately parallel to the *b*-axis.

As regards the Fe^{2+} component, the D doublet, which is associated with E on the same crystallographic site, can then be attributed to the Fe(1) site with calculated $QS^l_D = 0.90(4)$ mm s^{-1} and $\eta_D = 0.4$. Therefore, Fe(1) presents a mixed-valence situation, while the trigonal bipyramidal Fe(2) and Fe(3) are pure Fe^{2+} sites, in agreement with the bond valence sum calculations.

To attribute two other major components, A and B, to the Fe(2) and Fe(3) sites, we need to introduce both the QS^l and QS^V terms in the discussion. However, the lack of information about the electronic configuration of Fe^{2+} in this structure with low symmetry does not allow us to calculate the QS^V terms. Consequently, we have only performed QS^l calculations at the Fe(2) and Fe(3) sites. For Fe(2), limited to the first oxygen neighbors, $QS^l_2 = +2.02(12)$ mm s^{-1} and $\eta_2 = 0.8(1)$, while for Fe(3), smaller values for both parameters were obtained ($QS^l_3 = 1.76(14)$ mm s^{-1} and $\eta_3 = 0.6(1)$). We can conclude that the trigonal bipyramidal Fe(2) site is more distorted than Fe(3). Moreover, the consideration of the atom groups such as PO_4, water oxygen, hydroxo oxygen, etc., linked to the first oxygen neighbors of these two sites shows that Fe(3) has a simpler environment than Fe(2), which is consistent with the above lattice EFG results.

Concerning the assessment of QS^V, it must be noted that these terms, as the experimental QS ones, can be either positive or negative depending on the crystal field level scheme of Fe^{2+} and on the thermal population of these levels (the upper limit of $|QS^V|$ for a free Fe^{2+} ion is about 4.4 mm s^{-1}). Taking into account the possibilities of positive and negative experimental QS values for A and B, we have deduced QS^V_A and QS^V_B by subtracting the calculated $QS^l_{2\text{ or }3}$ with both in two possible positions: A is in Fe(2) and B in Fe(3) or vice versa. The calculations lead to the following considerations:

(17) Gütlich, P.; Link, R.; Trautwein, A. *Inorganic Chemistry Concepts, Volume 3: Mössbauer Spectroscopy and Transition Metal Chemistry*; Springer-Verlag: Berlin, 1978.

(18) Sternheimer, R. M. *Phys. Rev.* **1963**, *130*, 1423.

(i) If QS_A and QS_B are positive, the corresponding QS^V_A and QS^V_B have too small values (0.04−0.57 mm s^{-1}) which are not realistic in such distorted sites as Fe(2) or Fe(3). If QS_A and QS_B are negative, we obtain reasonable values (−3.56 to −4.35 mm s^{-1}) for the valence terms. A Mössbauer study in the magnetic state, namely, at low temperature, would allow us to verify these negative signs. (ii) From the lattice gradient $|QS^l_2| > |QS^l_3|$, one can assume that the symmetry of the coordination environment has a determinant influence on the symmetry of the $3d^6$ electron cloud around Fe^{2+} ions in the trigonal bipyramidal Fe(2) and Fe(3) sites. Therefore, this would indicate $|QS^V_2| > |QS^V_3|$, and the only assignment consistent with this argument corresponds to A in the Fe(3) sites and B+C in the Fe(2) sites ($QS^V_A = QS^V_3 = -3.56$ mm s^{-1}; $QS^V_B = QS^V_2 = -4.35$ mm s^{-1}).

In conclusion, the EFG calculations based on the room-temperature Mössbauer measurements confirm the presence of the mixed-valence iron at the octahedral site. They also allow correlation of the Mössbauer components with the crystallographic sites and provide information on the local symmetry of the iron sites.

Conclusions

This work illustrates that the structures and the compositions of the products of hydrothermal synthesis can be influenced by the reaction conditions. Reducing the amount of H_3PO_4 in the reaction mixture leads to a monoprotonated diamine template incorporated in the structure and to a lower HPO_4/PO_4 ratio in the prepared compounds. In addition, by comparison with the compound prepared previously,[12] we demonstrate that solvent plays an important role in hydrothermal (solvothermal) syntheses. A mixture of ethylene glycol and water, compared with a purely aqueous environment, has the following properties: (i) higher viscosity, which facilitates growth of single crystals; (ii) smaller polarity, which prevents inorganic ions from being trapped in "solvent cages" and thus increases their reactivity; (iii) a more reducing environment, as indicated from the fact that the mixed-valence compounds were also obtained, with smaller yield, even when only $FeCl_3 \cdot 6H_2O$ was used in the reaction mixture. In contrast, only the trivalent iron compound, $(C_4H_{12}N_2)_2[Fe_6(HPO_4)_2(PO_4)_6(H_2O)_2] \cdot H_2O$, was obtained from a pure aqueous system.[12] In addition, a ratio of the Fe^{II} and Fe^{III} components in the starting mixture close to that in the product helps to increase the yield of the synthesis.

Acknowledgment. We thank the Institute of Chemistry, Academia Sinica, and the National Science Council (NSC87-2113-M-001-019) for support and Professor S.-L. Wang and Ms. F.-L. Liao at the National Tsing Hua University for X-ray intensity data collection.

Supporting Information Available: Complete tables of crystallographic conditions, atomic coordinates, anisotropic thermal parameters, and bond lengths and angles for **1** and **2** (7 pages); observed and calculated structure factors (11 pages). Ordering information is given on any current masthead page.

CM980082E